Assessing the Spatial Relationship Between Fixation and Foveal Specializations

Melissa A. Wilk[a], **Adam M. Dubis**[a,1], **Robert F. Cooper**[b,2], **Phyllis Summerfelt**[c], **Alfredo Dubra**[a,b,c,d], and **Joseph Carroll**[a,b,c,d]

[a]Department of Cell Biology, Neurobiology, & Anatomy, Medical College of Wisconsin, 8701 Watertown Plank Road, Milwaukee, WI 53226, USA

[b]Department of Biomedical Engineering, Marquette University, 1250 W Wisconsin Avenue, Milwaukee, WI 53233, USA

[c]Department of Ophthalmology, Medical College of Wisconsin, 925 N. 87th Street, Milwaukee, WI 53226, USA

[d]Department of Biophysics, Medical College of Wisconsin, 8701 Watertown Plank Road, Milwaukee, WI 53226, USA

Abstract

Increased cone photoreceptor density, an avascular zone (FAZ), and the displacement of inner retinal neurons to form a pit are distinct features of the human fovea. As the fovea provides the majority of our vision, appreciating if and how these anatomical specializations are related is important for understanding foveal development, normal visual function, and retinal disease. Here we evaluated the relationship between these specializations and their location relative to the preferred retinal locus of fixation (PRL). We measured foveal pit volume, FAZ area, peak cone density, and location of the PRL in 22 subjects with normal vision using optical coherence tomography and adaptive optics scanning light ophthalmoscopy. Foveal pit volume was positively correlated with FAZ area; however, peak cone density was not correlated with pit volume. In addition, there was no systematic offset of the location of any of these specializations relative to PRL, and there was no correlation between the magnitude of the offset from PRL and the corresponding foveal specialization measurements (pit volume, FAZ area, peak cone density). The standard deviation of our PRL measurements was consistent with previous measurements of fixational stability. These data provide insight into the sequence of events during foveal development and may have implications for visual function and retinal disease.

Corresponding Author: Joseph Carroll (jcarroll@mcw.edu).
[1]Present Address: UCL-Institute of Ophthalmology, University College London, 11-43 Bath Street, London EC1V 9EL, UK
[2]Present Address: Department of Psychology, University of Pennsylvania, Philadelphia, PA 19104, USA

Keywords

Foveal morphology; foveal pit; foveal avascular zone; cone density; fixation

1. INTRODUCTION

The normal fovea is a highly specialized region of the human retina, characterized by the foveal avascular zone (FAZ), complete displacement of inner retinal neurons (creating the characteristic foveal "pit"), increased cone packing, and an absence of rod photoreceptors (Hendrickson, 2005, Provis, Dubis, Maddess & Carroll, 2013). While the fovea itself represents a relatively small area of the retina, it drives the majority of our visual function. Developmental disruption of the fovea in conditions such as albinism, aniridia, isolated foveal hypoplasia, and premature birth are linked with a decrease in visual function throughout life (Nelson, Spaeth, Nowinski, Margo & Jackson, 1984, Quinn & Dobson, 1996, Summers, 1996). Likewise, alterations to the foveal region in adulthood by conditions such as diabetic retinopathy and age-related macular degeneration result in a similar reduction in vision (Cunha-Vaz, Ribeiro & Lobo, 2014, Zarbin, Casaroli-Marano & Rosenfeld, 2014). Examination of the different aspects of foveal specializations and how they are related to one another will aid in the understanding of the anatomical basis of visual dysfunction in such conditions, as well as clarify models of normal foveal development.

In addition, while many tests of visual function are intended to test central vision (i.e., at the fovea), the preferred retinal locus of fixation (PRL) is actually the target of many of these tests. However, it is not known how the PRL relates to the different foveal specializations. Putnam and colleagues (Putnam, Hofer, Doble, Chen, Carroll & Williams, 2005) have shown that the PRL is offset from the location of peak cone density by about 50 microns, with no consistency in the direction of offset across the five subjects tested. However, this study only assessed fixation relative to the cone mosaic, not the FAZ or pit. It remains to be seen how the PRL is associated with other features of the fovea.

Due to the heterogeneity in methods of defining and assessing foveal morphology, it is also important to understand the relationships between each of the existing foveal measurements. Here we suggest metrics for objective quantification of foveal pit size, avascular area, and photoreceptor mosaic specialization, and examine the relationships between them. In addition, we evaluated the location of each specialization (center of FAZ, bottom of pit, and location of peak cone density) relative to the PRL. The quantification of these metrics and relationships will allow better comparison of foveal morphology across studies and could provide an improved understanding of visual function and retinal development and disease.

2. METHODS

2.1 Subjects

This study followed the tenets of the Declaration of Helsinki and was approved by the Medical College of Wisconsin Institutional Review Board. Written informed consent was obtained from all subjects (or an adult guardian for minors) after explanation of the nature

and possible consequences of the study. Twenty-two subjects (6 female, 16 male) aged 13–67 years (average ± standard deviation = 31 ± 16 years) were recruited to participate in this study (Table 1). Subjects with refractive error of 10 diopters or more, or with other vision-limiting pathology were excluded from the study. Subjects' self-reported ethnicities were Asian (n = 2), African American (n = 2), or Caucasian (n = 18). For the imaging experiments, each subject had one eye dilated and accommodation suspended using one drop each of Phenylephrine Hydrochloride (2.5%) and Tropicamide (1%). Axial length, used for calibrating the lateral scale of all retinal images, was measured using an IOL Master (Carl Zeiss Meditec, Dublin, CA).

2.2 Quantifying Foveal Pit Metrics

Volumetric images of the macula were acquired using the Cirrus High Definition (HD)-OCT (Cirrus HD-OCT; Carl Zeiss Meditec, Dublin, CA). Volume scans were nominally 6×6 mm (assuming a 24.46 mm axial length) and consisted of 128 B-scans (512 A-scans/B-scan). Foveal pit volume was calculated from topographical maps of retinal thickness as previously described (Wilk, McAllister, Cooper, Dubis, Patitucci, Summerfelt, Anderson, Stepien, Costakos, Connor, Wirostko, Chiang, Dubra, Curcio, Brilliant, Summers & Carroll, 2014). The bottom of the pit was located using the automatic "Fovea Finder" of the Cirrus software.

2.3 Assessing the Foveal Avascular Zone (FAZ)

Subjects' FAZs were imaged using OCT Angiography (RTVue XR 100 Avanti, Optovue, Inc., Fremont, CA; nine subjects), adaptive optics scanning light ophthalmoscopy (AOSLO; 11 subjects), or the Retinal Function Imager (RFI, Optical Imaging Ltd., Rehovat, Israel; two subjects). When possible, multiple OCT Angiography images were acquired, aligned, and averaged in ImageJ to achieve better signal-to-noise ratio (Schneider, Rasband & Eliceiri, 2012, Thévenaz, Ruttimann & Unser, 1998) (Fig. 1A). AOSLO images were registered and averaged as previously described (Cooper, Dubis, Pavaskar, Rha, Dubra & Carroll, 2011, Dubra & Harvey, 2010) prior to manual montaging in Photoshop (Adobe Systems, San Jose, CA). For all imaging modalities, the boundaries of the FAZ were manually identified by a single observer (MAW) using ImageJ (Schneider et al., 2012) (Fig. 1A). A mask was then constructed from the identified boundary points to create a closed contour defining the FAZ (Fig. 1B) using MATLAB software (Mathworks, Natick, MA). The area of the FAZ was calculated by multiplying the area (mm^2) of one pixel, adjusting for ocular magnification, by the number of pixels encompassed by the mask. Similarly, the perimeter of the FAZ in millimeters was also computed from the mask. Acircularity was defined as the ratio of FAZ perimeter to the circumference of a circle with an area equal to that of the FAZ, as previously described (Tam, Dhamdhere, Tiruveedhula, Manzanera, Barez, Bearse, Adams & Roorda, 2011). In this approach, an acircularity of 1 corresponds to a perfect circle, and values greater than 1 indicate an increasingly oblong or irregular shape.

2.4 Measuring Peak Cone Density

Confocal reflectance AOSLO images of the foveal cone mosaic were registered and montaged as described in Section 2.3. Peak cone density was estimated as previously described (Wilk et al., 2014). To summarize this method, a region encompassing the peak density was cropped from the montage. Each cone in the image was identified using semi-

automated software (Garrioch, Langlo, Dubis, Cooper, Dubra & Carroll, 2012), and the density at each pixel in the image was computed by counting the cones within variable window sizes. The densities at each pixel for all window sizes were averaged, and the pixel with the greatest average density was deemed the location of peak density; this method is effectively similar to using a low-pass filter. The density at this location of peak density was then measured over a 37×37 μm sampling window for comparison to histology (Curcio, Sloan, Kalina & Hendrickson, 1990).

2.5 Determining the Preferred Retinal Locus of Fixation (PRL)

We used the AOSLO image sequences to determine the PRL (Supplemental Fig. 1). First, subjects were instructed to fixate on each of the four corners of the 1°- or 1.5°-wide AOSLO imaging raster. This allowed us to collect four AOSLO image sequences from equidistant naso-superior, temporo-superior, naso-inferior, and temporo-inferior locations relative to the center of fixation. The four image sequences were registered by rigid translation to a manually-selected reference frame to maximize their normalized cross-correlation (Cooper et al., 2011, Dubra & Harvey, 2010), and the central pixel of each frame was tracked. Frames with a minimum of approximately 30% overlap with the reference frame were considered for registration, thereby excluding frames with partial blinks, significant motion artifacts, or large drifts. For each set of four registered sequences, the same number of frames were registered and averaged at each location to ensure equal weighting when calculating the center of mass. Images from the four locations were montaged to map the inferred fixation loci from each imaging location in a single coordinate space. These×and y values were averaged to determine the center of mass of the inferred fixation loci (x_c, y_c), which was then considered the location of the PRL.

2.6 Calculating the Offset of Specializations Relative to PRL

Images of the foveal pit, FAZ, and PRL were manually aligned to the cone mosaic in Photoshop (Adobe Systems Incorporated, San Jose, CA) by a single observer (MAW). Because functional measures of vision are generally anchored by the location of fixation, we chose to use the PRL as our reference point. The retinal location of each of the three foveal specializations (peak density, pit center, and FAZ center) was determined relative to the PRL.

3. RESULTS

3.1 Variability in Foveal Specializations

We quantified common metrics of foveal morphology: pit volume, FAZ area, and peak cone density, finding that these were highly variable across subjects (Table 1, Fig. 2). Pit volume ranged from 0.021 to 0.18 mm^3 (mean ± standard deviation = 0.081 ± 0.038 mm^3), corresponding to an approximately 8.5-fold range in pit volume, which is less than the 11-fold variability previously reported (Wilk et al., 2014). However, the sample size here is smaller (22 versus 64), and only two subjects here were of African descent, a population known to have larger foveal pits than Caucasian subjects (Wagner-Schuman, Dubis, Nordgren, Lei, Odell, Chiao, Weh, Fischer, Sulai, Dubra & Carroll, 2011). Therefore, our data seem consistent with previously studies.

FAZ area was shown to range from 0.063 to 0.49 mm^2 (mean ± standard deviation = 0.24 ± 0.10 mm^2), a nearly 8-fold span, in agreement with previous reports (Bradley, Applegate, Zeffren & van Heuven, 1992, Chui, VanNasdale, Elsner & Burns, 2014, Chui, Zhong, Song & Burns, 2012, Popovic, Knutsson, Thaung, Owner-Peterson & Sjöstrand, 2011). Perimeter values ranged from 1.24 to 2.68 mm (mean ± standard deviation = 2.07 ± 0.39 mm), with acircularity values ranging from 1.08 to 1.56 (1.25 ± 0.15), indicating substantial variation in FAZ shape. The variability of FAZ shape across subjects is illustrated in Fig. 2.

Maximum cone density ranged from 106,700 to 214,000 cones/mm^2 (mean ± standard deviation = 145,900 ± 26,900 cones/mm^2). This two-fold range is consistent with previous in vivo studies (Li, Tiruveedhula & Roorda, 2010, Putnam et al., 2005, Wilk et al., 2014, Zhang, Godara, Blancob, Griffin, Wang, Curcio & Zhang, 2015) but lower than the range reported in histology (Curcio et al., 1990).

3.2 Relationship Between Foveal Specializations

Two relationships among the foveal specializations are of particular interest due to the implications for development: the link between FAZ and pit volume, and the relationship between pit volume and cone density. Studies of foveal development suggest that the FAZ is required for formation of a foveal pit (Provis, Diaz & Dreher, 1998, Provis, Sandercoe & Hendrickson, 2000, Springer & Hendrickson, 2004, Tick, Rossant, Ghorbel, Gaudric, Sahel, Chaumet-Riffaud & Paques, 2011). In addition, no vasculature should be found in the area devoid of inner retinal layers, so the FAZ boundary should never be smaller than this region of the pit (Tick et al., 2011). As such, we would expect there to be a strong relationship between the size of the FAZ and that of the pit. Consistent with this, we found that the pit volume was significantly correlated with FAZ area in our subjects (Spearman's rank correlation coefficient, $r_s = 0.73$, $p < 0.0001$; Fig. 3A).

Recently, we proposed that cone packing at the fovea did not require a foveal pit, as seen in subjects with albinism; however, additional cone packing may be facilitated by the presence of a pit, contrary to previous models of development (Wilk et al., 2014). While subjects with albinism that had pits also had higher peak cone densities, the peak cone density in these subjects was still quite variable (Wilk et al., 2014). These data would suggest that there might not be a strong relationship between peak cone density and pit size in the normal population, and our data support this hypothesis (peak cone density versus pit volume: $r_s = 0.032$, $p = 0.9$; Fig. 3B).

3.3 Location of Foveal Specializations

The location of each specialization relative to the PRL varied across subjects (Table 2; Figs. 4 & 5). The average (± standard deviation, range) distance between the PRL and the FAZ center was 61 μm (± 31 μm, range 9.5 – 120 μm). Nine subjects had FAZ centers temporo-inferior to the PRL, five were temporo-superior, five were naso-superior, and three were naso-inferior. The bottom of the pit was offset by 7.2 to 177 μm (mean ± standard deviation = 80 ± 38 μm) relative to PRL. In 10 subjects, the pit was temporo-inferior to the PRL, eight were temporo-superior, three were naso-superior, and one was naso-inferior. The location of peak cone density was offset by an average of 63 ± 50 μm (range 20 – 263 μm). It fell

temporo-inferior to the PRL in eight subjects, temporo-superior in seven, naso-inferior in four, and naso-superior in three subjects.

There was no consistent pattern in the proportion that each metric's offset contributed to the total offset across subjects (Fig. 5A). We wondered if the offset of each specialization would be related to the magnitude of the metrics; however, there was no relationship between the offset of individual specializations relative to PRL and the corresponding metric value (FAZ: $r_s = -0.07$, $p = 0.8$; pit: $r_s = 0.30$, $p = 0.2$; and cone density: $r_s = -0.29$, $p = 0.2$; Fig. 5B–D).

Of note, the standard deviation of the fixation points was consistent with previous measures of fixational stability (Barlow, 1952, Putnam et al., 2005, Steinman, Haddad, Skavenski & Wyman, 1973). The fixation data for each subject can be seen in Supplemental Fig. 2.

4. DISCUSSION

4.1 Implications

From our data, no clear spatial relationship exists among foveal specializations and PRL. As such, tests of visual function that rely on fixation are often not testing vision at the peak cone density, bottom of the pit, or center of the FAZ. This unpredictable organization complicates the issue of defining the fovea. While strictly speaking the fovea refers to the pit, it has been used to reference other specializations - e.g., location of peak cone density or PRL (Carroll, Neitz, Hofer, Neitz & Williams, 2004, Cooper et al., 2011, Wilk et al., 2014). The data presented here emphasize the importance in defining the true feature of interest rather than using the generic term "fovea".

Terminology aside, the results of this study have implications for current models of foveal development. There is a wealth of evidence supporting the presence of anti-angiogenic factors at the central retina, which likely induce formation of the FAZ (Kozulin, Natoli, Bumsted O'Brien, Madigan & Provis, 2010, Kozulin, Natoli, Bumsted O'Brien, Madigan & Provis, 2009, Kozulin, Natoli, C., Bumsted O'Brien & Provis, 2009, Provis et al., 2000). It has also been shown that the FAZ is formed prior to the foveal pit in monkeys (Hendrickson, Troilo, Possin & Springer, 2006, Provis et al., 2000). Modeling data from Springer and Hendrickson (Springer & Hendrickson, 2004) predicted that it is the absence of foveal vasculature in conjunction with intraocular pressure and growth-induced retinal stretch that gives rise to the primate foveal pit. In fact, their data suggested that without the FAZ, and subsequent altered elasticity, the passive forces of pressure and stretch could not generate a pit (Springer & Hendrickson, 2004). To further support this claim, several studies show a direct link between lack of a pit and lack of an FAZ in humans (Azuma, Nishina, Yanagisawa, Okuyama & Yamada, 1996, Marmor, Choi, Zawadzki & Werner, 2008, McGuire, Weinreb & Goldbaum, 2003, Walsh & Goldberg, 2007), and to our knowledge, no studies have shown presence of a pit in the absence of the FAZ (Provis et al., 2013). While foveal pit diameter appears to be unaffected by the size of the FAZ, there is evidence that smaller FAZs correlate with increased foveal thickness - i.e., shallower pits (Tick et al., 2011), in premature infants (Yanni, Wang, Chan, Carroll, Farsiu, Leffler, Spencer & Birch, 2012) and adults (Chui et al., 2012, Samara, Say, Khoo, Higgins, Magrath, Ferenczy & Shields, 2015). Furthermore, Dubis et al. found a significant correlation between FAZ area

and pit area, depth, and volume (Dubis, Hansen, Cooper, Beringer, Dubra & Carroll, 2012). Therefore, our data showing a significant correlation between pit volume and FAZ area are consistent with these data and with models suggesting a dependence of pit formation on the presence of the FAZ.

We recently proposed a hybrid model for foveal development which incorporates both active and passive aspects of foveal development to bring about increased cone packing at the fovea (Wilk et al., 2014). This model predicts that the presence of a pit facilitates additional cone packing, and in the absence of a foveal pit, cone packing occurs but is reduced. Our present data show no correlation between pit volume and peak cone density, suggesting that perhaps it is the presence of a pit, however small or incomplete, that allows for normal levels of cone packing to occur. However, there are cases of foveal hypoplasia in albinism in which peak cone density is normal or near normal (Wilk et al., 2014). It is, therefore, unclear what mechanism guides cone packing. Studies in macaque suggest gradients of FGF (fibroblast growth factor) are responsible for cone elongation at the fovea (Cornish, Madigan, Natoli, Hales, Hendrickson & Provis, 2005). Due to strong cell-cell associations, cones "stick together" as they elongate, thereby increasing cone density (Provis et al., 2013). It would be interesting to see if the FGF gradients also exist in the human retina, and if so, whether or not they are altered in cases of reduced cone packing. If these same gradients exist in the human albinotic retina, perhaps there is a more complex interplay between the passive and active models of foveal development than originally recognized. Future studies on these gradients in humans are needed to better understand this relationship.

4.2 Limitations

There are several limitations to this study. First, most subjects in this study are Caucasian. Since there are race-related differences in pit morphology (Wagner-Schuman et al., 2011), our limited number of African American and Asian subjects may not capture the true range of foveal morphology. Likewise, subjects with very high peak cone densities were excluded from this study, as the foveal cones could not confidently be identified due to the resolution limit of our current AOSLO. These factors limit the range of foveal morphology examined here, and alternative methods would be required to explore the full range of morphology that exists in the general population.

Another limitation is that three separate modalities were used to image the FAZ of our subjects. The resolution differences between devices could affect the defining of the FAZ. However, comparison of FAZ area measurements from two imaging modalities in the same subject yielded very similar data (average % difference in FAZ area = 6.5%), suggesting consistency between methods (Supplemental Table 1). Previous work by Dubis et al. (2012) also showed agreement in FAZ area values obtained with different techniques. Relatedly, different modalities (OCT and AOSLO) were used to image the various features of foveal morphology (FAZ, pit, and cone mosaic). The different images acquired were manually overlaid to assess the location of each specialization relative to the PRL. The alignment of different imaging modalities is a challenging, manual process and requires distinct landmarks, such as blood vessels, to approximate the position. The degree to which small errors in the alignment process affect the relationships examined here is unclear, though we

would not expect that the alignment would differ in relation to any of the foveal metrics, so it likely comes across as noise in our measurements.

An additional limitation in this study is the error in measuring PRL. Previous studies have shown that the size and shape of the fixation target affects the stability of fixation (McCamy, Najafian Jazi, Otero-Millan, Macknik & Martinez-Conde, 2013, Steinman, 1965, Thaler, Schütz, Goodale & Gegenfurtner, 2013). Here, we used a 1.0 or 1.5° red box (the illuminated raster in the AOSLO), and subjects were asked to fixate on the corners of the box. Presumably, attempts to fixate on the center of a large box would result in errors in locating the actual center. To evaluate this, we included a smaller dim box within the large box by modulating the scanner and imaged a small group of normal subjects (n = 10). Inclusion of the smaller target within the large box provided a PRL that more closely aligned with the average of the four corners and was significantly offset from the PRL as determined from the large target alone (data not shown). In addition, inclusion of the small target significantly improved fixation stability (reduced standard deviation of PRL) in the 10 subjects (data not shown). As such, analyzing only the four corners in our subjects likely mitigated this effect. However, this brief study brought to light other sources of errors in our measurement of PRL. First, our PRL measurements have been done using different versions of the AO ophthalmoscope with and without modulation of the imaging light source. When the modulation was on, the subject would see a dim outer edge extending approximately 40 pixels to one side of the imaging raster horizontally and 5–10 pixels to one side vertically; the presence of the dim edges could alter the chosen point of fixation if not clear which corner is the intended target. This shift in fixation would occur across all image sequences in that imaging session and corresponds to about 2 standard deviations in the fixation stability. While the offsets due to the light source modulation remain in our data, it is unlikely that their correction would change our results, given the non-preferential direction of the foveal specialization shifts relative to the PRL across subjects. However, knowing that these limitations exist, they should be accounted for in the future.

4.3 Conclusions

Here, we have shown that the location of the different foveal specializations is variably offset from the PRL. In addition, we've shown that pit volume is correlated with FAZ area, but not with peak cone density. These results have implications for models of foveal development, and more research into the mechanisms responsible for cone packing is required to better understand these relationships. Further exploration of the interactions between foveal specializations and fixation will provide insight that could be helpful in the development and targeting of therapies for retinal disease.

Supplementary Material

Refer to Web version on PubMed Central for supplementary material.

Acknowledgments

REFERENCES

Azuma N, Nishina S, Yanagisawa H, Okuyama T, Yamada M. PAX6 missense mutation in isolated foveal hypoplasia. Nature Genetics. 1996; 13(2):141–142. [PubMed: 8640214]

Barlow HB. Eye movements during fixation. Journal of Physiology. 1952; 116:290–306. [PubMed: 14939180]

Bradley A, Applegate RA, Zeffren BS, van Heuven WA. Psychophysical measurement of the size and shape of the human foveal avascular zone. Ophthalmic and Physiological Optics. 1992; 12(1):18–23. [PubMed: 1584610]

Carroll J, Neitz M, Hofer H, Neitz J, Williams DR. Functional photoreceptor loss revealed with adaptive optics: An alternate cause of color blindness. Proceedings of the National Academy of Sciences. 2004; 101(22):8461–8466.

Chui TYP, VanNasdale DA, Elsner AE, Burns SA. The association between the foveal avascular zone and retinal thickness. Investigative Ophthalmology & Visual Science. 2014; 55(10):6870–6877. [PubMed: 25270194]

Chui TYP, Zhong Z, Song H, Burns SA. Foveal avascular zone and its relationship to foveal pit shape. Optometry and Vision Science. 2012; 89(5):602–610. [PubMed: 22426172]

Cooper RF, Dubis AM, Pavaskar A, Rha J, Dubra A, Carroll J. Spatial and temporal variation of rod photoreceptor reflectance in the human retina. Biomedical Optics Express. 2011; 2(9):2577–2589. [PubMed: 21991550]

Cornish EE, Madigan MC, Natoli R, Hales A, Hendrickson AE, Provis JM. Gradients of cone differentiation and FGF expression during development of the foveal depression in macaque retina. Visual Neuroscience. 2005; 22(4):447–459. [PubMed: 16212702]

Cunha-Vaz J, Ribeiro L, Lobo C. Phenotypes and biomarkers of diabetic retinopathy. Progress in Retinal and Eye Research. 2014; 41(2014):90–111. [PubMed: 24680929]

Curcio CA, Sloan KR, Kalina RE, Hendrickson AE. Human photoreceptor topography. Journal of Comparative Neurology. 1990; 292(4):497–523. [PubMed: 2324310]

Dubis AM, Hansen BR, Cooper RF, Beringer J, Dubra A, Carroll J. Relationship between the foveal avascular zone and foveal pit morphology. Investigative Ophthalmology & Visual Science. 2012; 53(3):1628–1636. [PubMed: 22323466]

Dubra, A., Harvey, Z. Registration of 2D images from fast scanning ophthalmic instruments. In: Fischer, B.Dawant, B., Lorenz, C., editors. Biomedical Image Registration. Berlin: Springer-Verlag; 2010. p. 60-71.

Garrioch R, Langlo C, Dubis AM, Cooper RF, Dubra A, Carroll J. Repeatability of in vivo parafoveal cone density and spacing measurements. Optometry and Vision Science. 2012; 89(5):632–643. [PubMed: 22504330]

Hendrickson, A. Organization of the adult primate fovea. In: Penfold, PL., Provis, JM., editors. Macular Degeneration. Heidelberg: Springer-Verlag; 2005. p. 1-20.

Hendrickson A, Troilo D, Possin D, Springer A. Development of the neural retina and its vasculature in the marmoset monkey *Callithrix jacchus*. Journal of Comparative Neurology. 2006; 497(2):270–286. [PubMed: 16705674]

Kozulin P, Natoli R, Bumsted O'Brien KM, Madigan MC, Provis J. The cellular expression of antiangiogenic factors in fetal primate macula. Investigative Ophthalmology & Visual Science. 2010; 51(8):4298–4306. [PubMed: 20357200]

Kozulin P, Natoli R, Bumsted O'Brien KM, Madigan MC, Provis JM. Differential expression of anti-angiogenic factors and guidance genes in the developing macula. Molecular Vision. 2009; 15:49–59.

Kozulin P, Natoli R, C MM, Bumsted O'Brien KM, Provis JM. Gradients of Eph-A6 expression in primate retina suggest roles in both vascular and axon guidance. Molecular Vision. 2009; 15:2649–2662. [PubMed: 20011078]

Li KY, Tiruveedhula P, Roorda A. Intersubject variability of foveal cone photoreceptor density in relation to eye length. Investigative Ophthalmology & Visual Science. 2010; 51(12):6858–6867. [PubMed: 20688730]

Marmor MF, Choi SS, Zawadzki RJ, Werner JS. Visual insignificance of the foveal pit: Reassessment of foveal hypoplasia as fovea plana. Archives of Ophthalmology. 2008; 126(7):907–913. [PubMed: 18625935]

McCamy MB, Najafian Jazi A, Otero-Millan J, Macknik SL, Martinez-Conde S. The effects of fixation target size and luminance on microsaccades and square-wave jerks. PeerJ. 2013; 1:e9. [PubMed: 23638403]

McGuire DE, Weinreb RN, Goldbaum MH. Foveal hypoplasia demonstrated in vivo with optical coherence tomography. American Journal of Ophthalmology. 2003; 135(1):112–114. [PubMed: 12504716]

Nelson LB, Spaeth GL, Nowinski TS, Margo CE, Jackson L. Aniridia. A review. Survey of Ophthalmology. 1984; 28(6):621–642. [PubMed: 6330922]

Popovic Z, Knutsson P, Thaung J, Owner-Peterson M, Sjöstrand J. Noninvasive imaging of human foveal capillary network using dual-conjugate adaptive optics. Investigative Ophthalmology & Visual Science. 2011; 52(5):2649–2655. [PubMed: 21228372]

Provis JM, Diaz CM, Dreher B. Ontogeny of the primate fovea: A central issue in retinal development. Progress in Neurobiology. 1998; 54(5):549–581. [PubMed: 9550191]

Provis JM, Dubis AM, Maddess T, Carroll J. Adaptation of the central retina for high acuity vision: Cones, the fovea, and the avascular zone. Progress in Retinal and Eye Research. 2013; 35:63–81. [PubMed: 23500068]

Provis JM, Sandercoe T, Hendrickson AE. Astrocytes and blood vessels define the foveal rim during primate retinal development. Investigative Ophthalmology & Visual Science. 2000; 41(10):2827–2836. [PubMed: 10967034]

Putnam NM, Hofer HJ, Doble N, Chen L, Carroll J, Williams DR. The locus of fixation and the foveal cone mosaic. Journal of Vision. 2005; 5(7):632–639. [PubMed: 16231998]

Quinn GE, Dobson V. Outcome of prematurity and retinopathy of prematurity. Current Opinion in Ophthalmology. 1996; 7(3):51–56. [PubMed: 10163460]

Samara WA, Say EA, Khoo CT, Higgins TP, Magrath G, Ferenczy S, Shields CL. Correlation of foveal avascular zone size with foveal morphology in normal eyes using optical coherence tomography angiography. Retina. 2015; 35(11):2188–2195. [PubMed: 26469536]

Schneider CA, Rasband WS, Eliceiri KW. NIH Image to ImageJ: 25 years of image analysis. Nature Methods. 2012; 9(7):671–675. [PubMed: 22930834]

Springer AD, Hendrickson AE. Development of the primate area of high acuity. 1. Use of finite element analysis models to identify mechanical variables affecting pit formation. Visual Neuroscience. 2004; 21:53–62. [PubMed: 15137581]

Steinman RM. Effect of target size, luminance, and color on monocular fixation. Journal of the Optical Society of America. 1965; 55(9):1158–1165.

Steinman RM, Haddad GM, Skavenski AA, Wyman D. Miniature eye movement. Science. 1973; 181(4102):810–819. [PubMed: 4198903]

Summers CG. Vision in albinism. Transactions of the American Ophthalmological Society. 1996; 94:1095–1155. [PubMed: 8981720]

Tam J, Dhamdhere KP, Tiruveedhula P, Manzanera S, Barez S, Bearse MA Jr, Adams AJ, Roorda A. Disruption of the retinal parafoveal capillary network in type 2 diabetes before the onset of diabetic retinopathy. Investigative Ophthalmology & Visual Science. 2011; 52(12):9257–9266. [PubMed: 22039250]

Thaler L, Schütz AC, Goodale MA, Gegenfurtner KR. What is the best fixation target? The effect of target shape on stability of fixational eye movements. Vision Research. 2013; 76:31–42. [PubMed: 23099046]

Thévenaz P, Ruttimann UE, Unser M. A pyramid approach to subpixel registration based on intensity. IEEE Transactions on Image Processing. 1998; 7(1):27–41. [PubMed: 18267377]

Tick S, Rossant F, Ghorbel I, Gaudric A, Sahel JA, Chaumet-Riffaud P, Paques M. Foveal shape and structure in a normal population. Investigative Ophthalmology & Visual Science. 2011; 52(8): 5105–5110. [PubMed: 21803966]

Wagner-Schuman M, Dubis AM, Nordgren RN, Lei Y, Odell D, Chiao H, Weh E, Fischer W, Sulai Y, Dubra A, Carroll J. Race- and sex-related differences in retinal thickness and foveal pit morphology. Investigative Ophthalmology & Visual Science. 2011; 52(1):625–634. [PubMed: 20861480]

Walsh MK, Goldberg MF. Abnormal foveal avascular zone in nanophthalmos. American Journal of Ophthalmology. 2007; 143(6):1067–1068. [PubMed: 17524786]

Wilk MA, McAllister JT, Cooper RF, Dubis AM, Patitucci TN, Summerfelt P, Anderson JL, Stepien KE, Costakos DM, Connor TB Jr, Wirostko WJ, Chiang PW, Dubra A, Curcio CA, Brilliant MH, Summers CG, Carroll J. Relationship between foveal cone specialization and pit morphology in albinism. Investigative Ophthalmology & Visual Science. 2014; 55(7):4186–4198. [PubMed: 24845642]

Yanni SE, Wang J, Chan M, Carroll J, Farsiu S, Leffler JN, Spencer R, Birch EE. Foveal avascular zone and foveal pit formation after preterm birth. British Journal of Ophthalmology. 2012; 96(7): 961–966. [PubMed: 22544530]

Zarbin MA, Casaroli-Marano RP, Rosenfeld PJ. Age-related macular degeneration: Clinical findings, histopathology and imaging techniques. Developments in Ophthalmology. 2014; 53:1–32. [PubMed: 24732758]

Zhang T, Godara P, Blancob ER, Griffin RL, Wang X, Curcio CA, Zhang Y. Variability in human cone topography assessed by adaptive optics scanning laser ophthalmoscopy. American Journal of Ophthalmology. 2015; 160(2):290–300. [PubMed: 25935100]
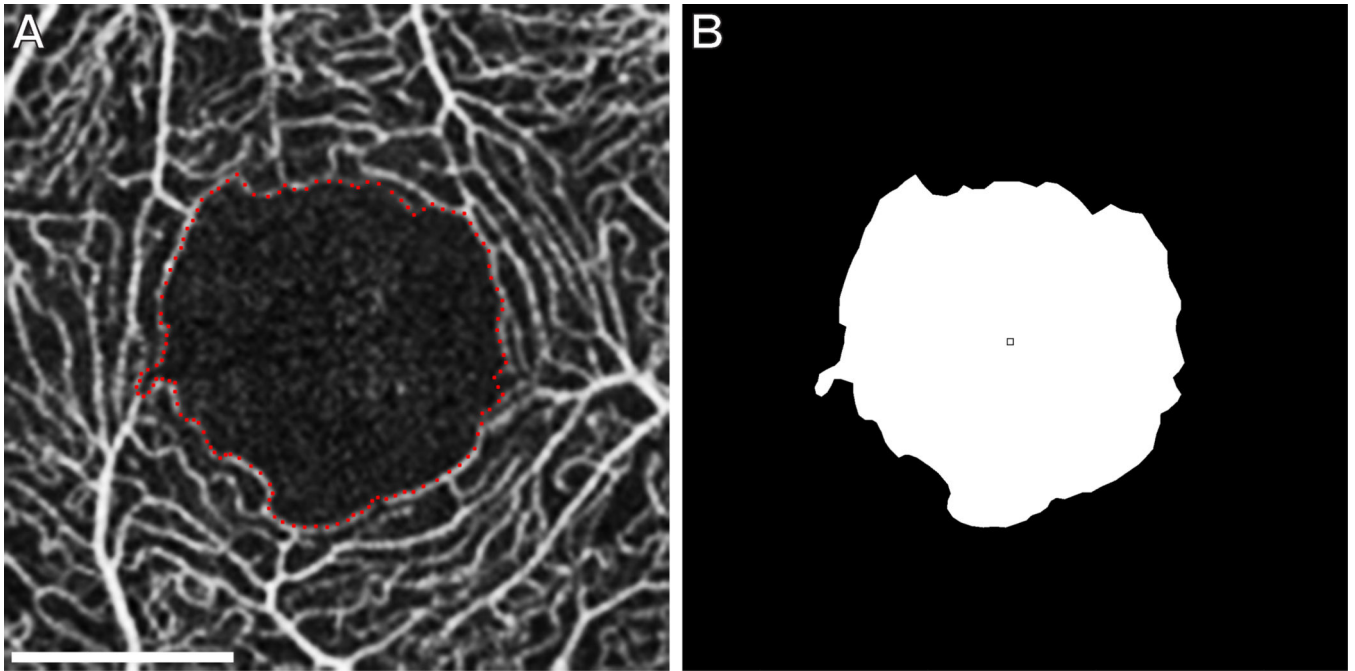
Fig. 1.
Calculating FAZ area and perimeter. (A) Foveal avascular zone image acquired using OCT angiography showing the manual segmentation at the FAZ boundary (red dots). (B) Using the coordinates selected in (A) and interpolating between points, a mask of the FAZ was created. The boundary coordinates (junction of black and white areas) comprise the FAZ perimeter. All points within the boundary coordinates (white area) comprise the FAZ area. The square denotes the center of mass for the FAZ mask. Scale bar = 500 μm.
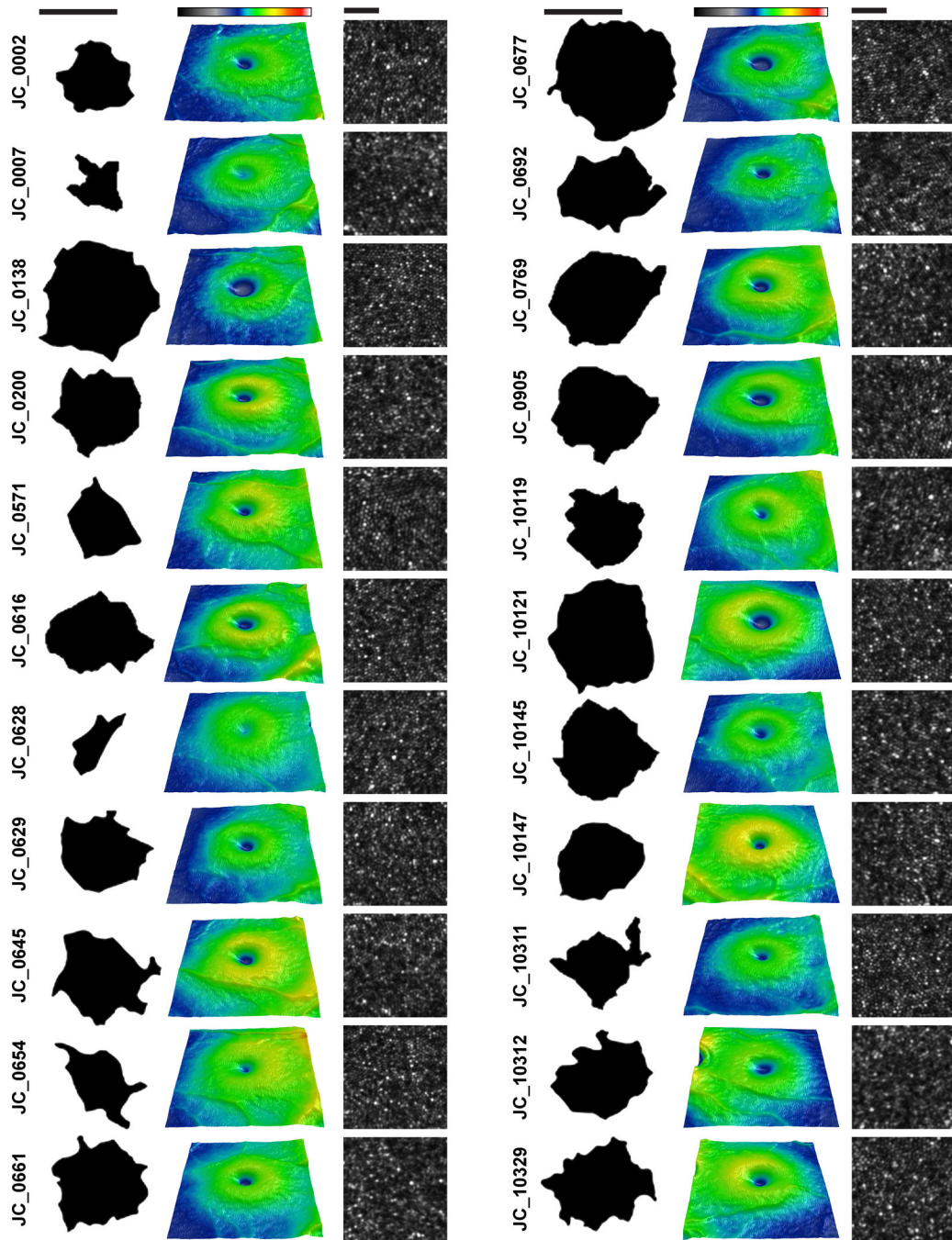
Fig. 2.
FAZ masks, retinal thickness maps, and foveal cone images are shown for each subject. The left panel for each column shows the mask created from FAZ segmentation and highlights the variability in FAZ size and shape. FAZ scale bars = 500 μm. The middle panel displays the retinal thickness map from the Cirrus HD-OCT (black = 0 μm, white = 500 μm). Scans are nominally 6 × 6 mm, though the actual size varies due to individual differences in axial length. Not that pit volume was derived from thickness data after the lateral scale was corrected for axial length differences. Differences in pit shape can easily be appreciated.

Foveal cones mosaics, shown in the right panel, have been contrast adjusted for display. Foveal cone scale bars = 25 μm.

Fig. 3.
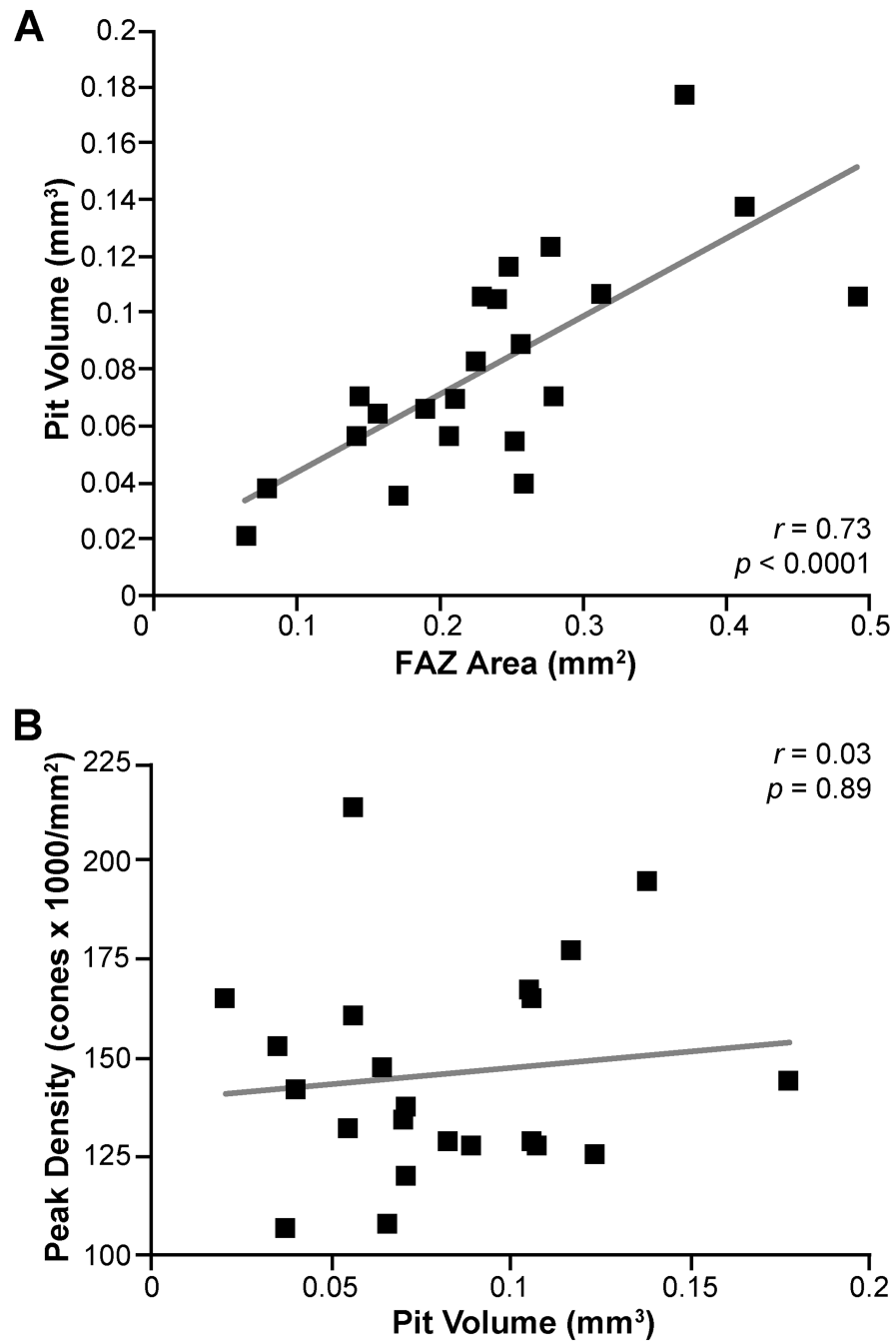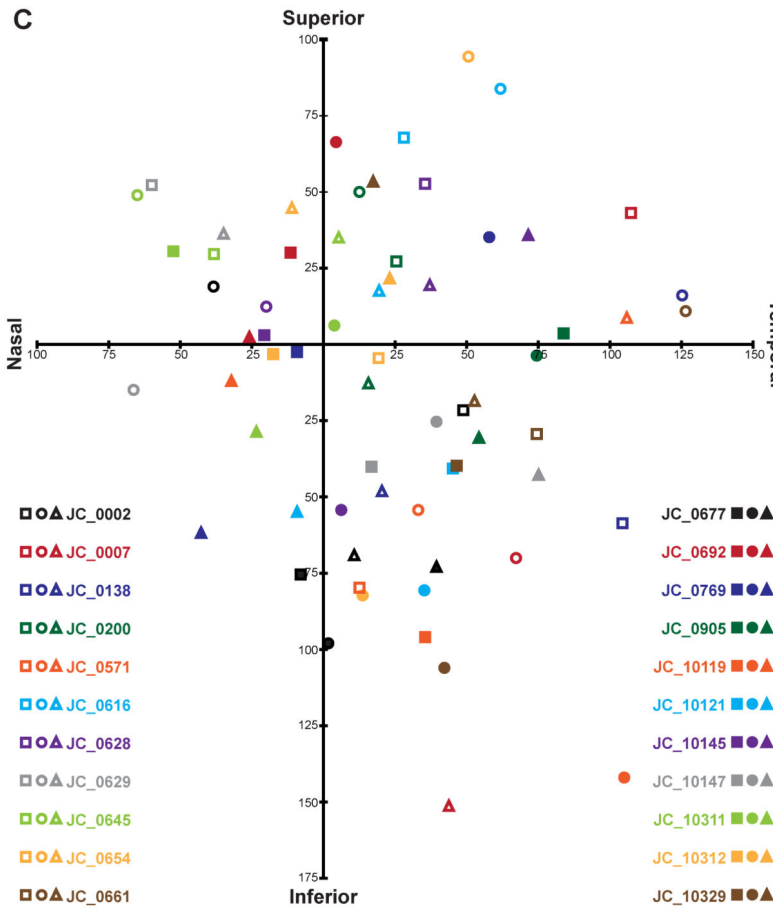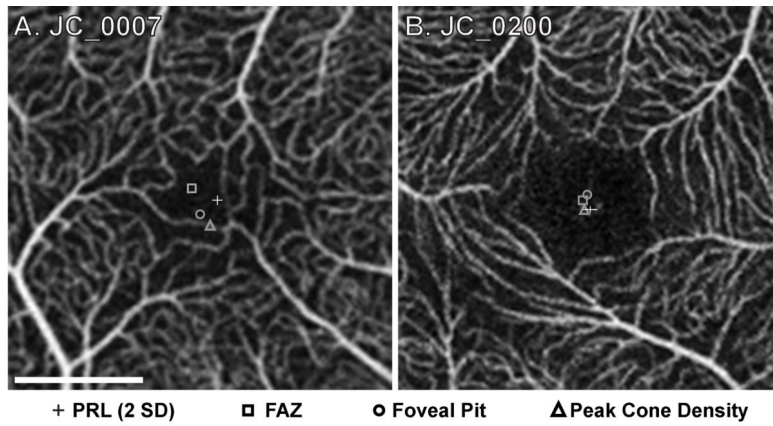Relationship between FAZ, pit, and peak cone density. (A) Pit volume is significantly correlated with FAZ area ($p < 0.0001$; Spearman Rank Correlation). (B) Peak cone density is not significantly correlated with pit volume ($p = 0.9$; Spearman Rank Correlation).

Fig. 4.

The co-localization of the location of peak cone density, FAZ, pit, and PRL varies across subjects. FAZ images acquired with OCT angiography for a subject with a small FAZ but large offset between the foveal specializations and PRL (A, JC_0007), and a subject with average FAZ area and close co-localization of foveal specializations and PRL (B, JC_0200). Crosses denote the average PRL, with the length of the lines representing 2 standard deviations in PRL for the horizontal and vertical directions. Squares correspond to the FAZ center, circles represent the bottom of the foveal pit, and triangles mark the location of peak

cone density. Scale bar = 500 μm. C) A scatter plot illustrates the non-preferential direction offset of each specialization from the PRL in each subject. Squares, circles, and triangles again represent the FAZ center, bottom of the foveal pit, and location of peak cone density, respectively.
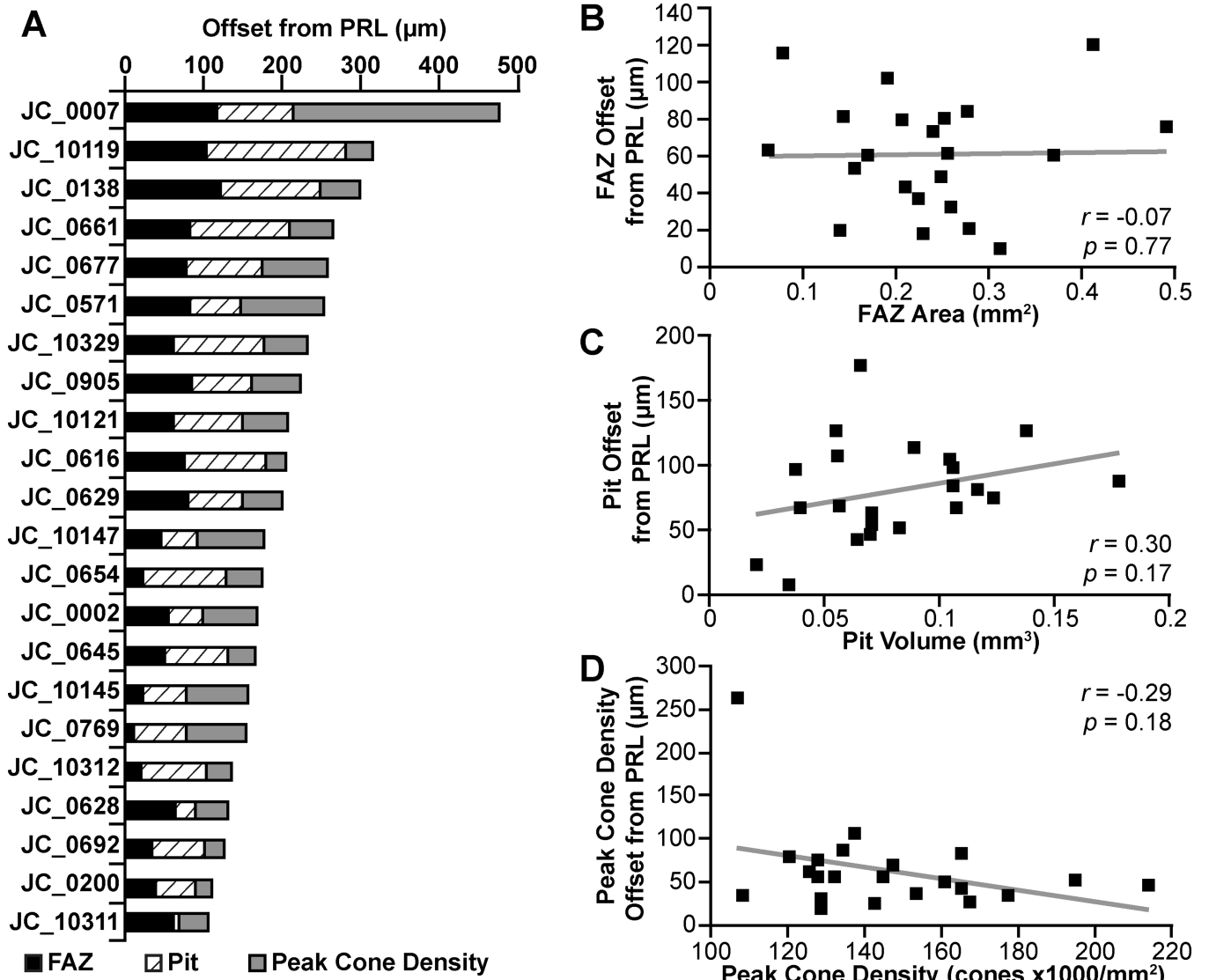
Fig. 5.
Specialization offsets from PRL. (A) The location of each specialization (FAZ, pit, peak cone density) was determined relative to PRL (raw values shown in Fig. 4C). Subjects are ranked from the greatest cumulative offset (top) to closest clustering of specializations (bottom). There is no consistency in the contribution of each specialization to the total offset across subjects. (B–D) The offset of each specialization was not correlated with the magnitude of that specialization (FAZ area, pit volume, or peak cone density).

Subject demographics and foveal metrics

Table 1

Subject	Age	Sex	Ethnicity	Eye	Axial Length (mm)	Method for FAZ	FAZ Area (mm²)	FAZ Perimeter (mm)	Pit Volume (mm³)	Peak Cone Density (cones/mm²)	Horizontal SD of PRL (µm)	Vertical SD of PRL (µm)	Number of Frames for PRL*
JC_0002	28	M	Caucasian	OD	24.72	RFI	0.1558	1.635	0.0641	147,550	15.7	18.4	90
JC_0007	37	M	Caucasian	OD	27.45	OCTA	0.0788	1.375	0.0375	106,650	19.2	17.1	103
JC_0138	25	F	Asian	OD	22.75	RFI	0.4110	2.613	0.1374	195,030	12.2	14.7	105
JC_0200	26	M	Caucasian	OD	24.72	OCTA	0.2242	1.902	0.0826	128,560	19.74	11.5	144
JC_0571	25	M	Caucasian	OD	24.08	AO	0.1428	1.570	0.0706	137,330	15.8	9.2	95
JC_0616	23	M	Caucasian	OD	24.35	OCTA	0.2394	1.997	0.1046	167,280	15.0	11.1	118
JC_0628	67	F	Caucasian	OD	22.92	AO	0.0634	1.243	0.0207	165,080	15.7	13.6	98
JC_0629	63	M	Caucasian	OD	23.29	AO	0.2068	1.976	0.0563	160,700	9.6	14.7	73
JC_0645	20	M	Caucasian	OD	23.76	AO	0.2480	2.525	0.1163	177,500	9.9	10.0	128
JC_0654	25	F	Caucasian	OD	23.57	AO	0.1405	2.049	0.0561	214,020	12.9	7.9	131
JC_0661	23	M	African American	OD	25.52	AO	0.2521	2.307	0.0549	132,210	16.4	13.2	76
JC_0677	24	F	Caucasian	OD	24.03	OCTA	0.4902	2.675	0.1060	165,080	9.4	10.7	131
JC_0692	40	M	Caucasian	OD	24.54	AO	0.2582	2.308	0.0400	142,440	19.7	11.6	87
JC_0769	21	F	Caucasian	OD	24.29	OCTA	0.3111	2.204	0.1068	127,830	15.9	10.8	118
JC_0905	21	M	Caucasian	OD	22.46	OCTA	0.2764	2.107	0.1231	125,640	15.8	14.3	87
JC_10119	22	M	Asian	OD	25.90	OCTA	0.1902	1.825	0.0657	108,110	19.7	14.0	120
JC_10121	23	M	African American	OS	23.93	AO	0.3692	2.389	0.1773	144,630	14.5	9.3	134
JC_10145	49	F	Caucasian	OD	24.66	OCTA	0.2784	2.104	0.0709	120,530	20.8	13.7	133
JC_10147	13	M	Caucasian	OS	24.66	AO	0.2105	1.771	0.0699	134,400	18.6	17.5	111
JC_10311	62	M	Caucasian	OD	22.86	OCTA	0.1698	2.282	0.0348	153,400	12.9	8.6	100
JC_10312	15	M	Caucasian	OS	26.88	AO	0.2284	2.172	0.1055	128,560	20.2	14.2	85
JC_10329	22	M	Caucasian	OS	24.46	AO	0.2548	2.504	0.0887	127,830	11.37	10.48	141

RFI = Retinal Function Imager; OCTA = OCT angiography; AO = adaptive optics scanning light ophthalmoscopy; OD = right eye; OS = left eye

*
Number of frames is per video location. Total number of fixation points is 4 times the number listed for each subject. The total number of frames recorded for each location, and thus the maximum possible fixation points per location, was 150 for each subject.

Table 2

Location of FAZ, pit, and peak cone density relative to PRL

Subject	FAZ	Pit	Peak Cone
JC_0002	48.9 T, 21.4 I	38.6 N, 18.9 S	10.7 T, 69.0 I
JC_0007	107.5 T, 43.3 S	67.4 T, 70.1 I	23.2 T, 262.0 I
JC_0138	104.5 T, 58.5 I	125.3 T, 16.1 S	20.4 T, 48.3 I
JC_0200	25.2 T, 27.2 S	12.6 T, 50.3 S	15.6 T, 12.6 I
JC_0571	12.6 T, 79.9 I	33.2 T, 54.2 I	106.0 T, 8.8 S
JC_0616	27.9 T, 67.7 S	61.8 T, 83.8 S	19.5 T, 17.8 S
JC_0628	35.5 T, 52.6 S	19.9 N, 12.4 S	37.1 T, 19.5 S
JC_0629	60.0 N, 52.3 S	66.4 N, 14.9 I	35.0 N, 36.2 S
JC_0645	38.2 N, 29.6 S	65.0 N, 48.9 S	5.3 T, 34.9 S
JC_0654	19.2 T, 4.5 I	50.7 T, 94.1 S	11.0 N, 44.6 S
JC_0661	74.5 T, 29.3 I	126.4 T, 11.1 S	52.8 T, 18.6 I
JC_0677	7.9 N, 75.4 I	1.6 T, 97.9 I	39.5 T, 72.7 I
JC_0692	11.4 N, 30.1 S	4.2 T, 66.5 S	25.8 N, 2.1 S
JC_0769	9.2 N, 2.4 I	57.9 T, 35.1 S	42.7 N, 61.5 I
JC_0905	83.9 T, 3.6 S	74.6 T, 3.6 I	54.3 T, 30.3 I
JC_10119	35.5 T, 96.0 I	104.9 T, 142.0 I	32.3 N, 11.7 I
JC_10121	45.2 T, 40.8 I	35.4 T, 80.5 I	9.3 N, 55.0 I
JC_10145	20.8 N, 3.0 S	6.1 T, 54.2 I	71.4 T, 35.9 S
JC_10147	16.7 T, 40.0 I	39.5 T, 25.3 I	75.0 T, 42.6 I
JC_10311	52.5 N, 30.5 S	3.8 T, 6.1 S	23.5 N, 28.6 I
JC_10312	17.5 N, 3.3 I	13.7 T, 82.1 I	23.0 T, 21.9 S
JC_10329	46.2 T, 39.7 I	42.2T, 106.1 I	17.1 T, 53.8 S

T = temporal; N = nasal; S = superior; I = inferior

All distances are in microns